10108 *Inorg. Chem.* **2010**, *49*, 10108–10116
DOI: 10.1021/ic101391x

Inorganic Chemistry
Article

Dinuclear Cu(II) Hypocrellin B Complexes with Enhanced Photonuclease Activity

Yi Sun,[†,‡] Yuan-Jun Hou,[†] Qian-Xiong Zhou,[†] Wan-Hua Lei,[†] Jing-Rong Chen,[†] Xue-Song Wang,[*,†] and Bao-Wen Zhang[*,†]

[†]*Key Laboratory of Photochemical Conversion and Optoelectronic Materials, Technical Institute of Physics and Chemistry, Chinese Academy of Sciences, Beijing 100190, P. R. China, and* [‡]*Graduate School of Chinese Academy of Sciences, Beijing 100049, P. R. China*

Received July 13, 2010

Five new dinuclear Cu(II) complexes were designed and synthesized, using hypocrellin B, a naturally occurring photosensitizer that has received extensive studies as promising photodynamic therapy (PDT) agent, as bridging ligand, and five kinds of diimine ligands, including 2,2′-bipyridine (bpy), 1,10-phenanthroline (phen), 3,4,7,8-tetramethyl-1,10-phenanthroline (tmp), dipyrido[3,2-*d*:2′,3′-*f*]quinoxaline (dpq), and dipyrido[3,2-*a*:2′,3′-*c*]phenazene (dppz), as terminal ligands, respectively. The Cu^{2+}-HB complexes exhibit improved water solubility, enhanced absorptivity in the phototherapeutic window of 600−900 nm, and increased binding affinity toward dsDNA than their parent HB. The biologically accessible redox potential of Cu(II)/Cu(I) couple renders the five Cu^{2+}-HB complexes chemical nuclease activities in the presence of reducing agent such as ascorbic acid. Moreover, the readily available redox potential of Cu(II)/Cu(I) couple switches the photodynamic activity from type II mechanism (singlet oxygen mechanism) for HB to type I mechanism (radical mechanism) for the Cu^{2+}-HB complexes. Of the five Cu^{2+}-HB complexes, complex **3**−**5** with terminal diimine ligands of tmp, dpq, and dppz, respectively, can photocleave supercoiled pBR322 DNA more efficiently than HB. These findings open a new avenue for the development of the HB derivatives with higher photodynamic activity and better clinical applicability.

1. Introduction

Hypocrellins, including hypocrellin A (HA) and hypocrellin B (HB), isolated from the fungus of hypocrella bambusae, are well-recognized as promising nonporphyrin photosensitizers for photodynamic therapy (PDT) application, because of their high singlet oxygen quantum yields, low aggregation tendency, and rapid metabolism in vivo.[1] Though presenting high photodynamic killing activity toward many kinds of tumor cell lines,[2] viruses,[3] and bacteria,[4] the clinical use of the natural hypocrellins is severely limited by their poor water solubility and low absorptivity in the phototherapeutic window (600−900 nm), which urged the evolvement of various hypocrellin derivatives, such as sulfonated HA,[5] glycosylated HB,[6] cyclodextrin-modified HB,[7] quaternary ammonium group-substituted HB,[8] and tyrosine-appended HB.[9] In this respect, the metal complexes of hypocrellins are very attractive because they can be prepared with simple procedures and the enhanced water solubility and improved absorptivity within the phototherapeutic window can be achieved simultaneously.[10] Moreover, the positively charged

*Corresponding author. Tel.: +86-10-82543592. Fax: +86-10-62564049. E-mail: xswang@mail.ipc.ac.cn (X.S.W.); g203@mail.ipc.ac.cn (B.W.Z.).

(1) (a) Diwu, Z. *Photochem. Photobiol.* **1995**, *61*, 529–539. (b) Diwu, Z.; Lown, J. W. *Photochem. Photobiol.* **1990**, *52*, 609–616.

(2) (a) Ali, S. M.; Chee, S. K.; Yuen, G. Y.; Olivo, M. *J. Photochem. Photobiol., B* **2001**, *65*, 59–73. (b) Zhang, J.; Cao, E. H.; Li, J. F.; Zhang, T. C. *J. Photochem. Photobiol., B* **1998**, *43*, 106–111.

(3) (a) Hirayama, J.; Ikebuchi, K.; Abe, H.; Kwon, K. W.; Ohnishi, Y.; Horiuchi, M.; Shinagawa, M.; Ikuta, K.; Kamo, N.; Sekiquchi, S. *Photochem. Photobiol.* **1997**, *66*, 697–700. (b) Kraus, G. A.; Zhang, W.; Fehr, M. J.; Petrick, J. W.; Wannemuehler, Y.; Carpenter, S. *Chem. Rev.* **1996**, *96*, 523–536. (c) Fehr, M. J.; Carpenter, S. L.; Wannemuehler, Y.; Petrich, J. W. *Biochem.* **1995**, *34*, 15845–15848. (d) Hudson, J. B.; Zhou, J.; Harris, L.; Yip, L.; Towers, G. H. N. *Photochem. Photobiol.* **1994**, *60*, 253–255.

(4) Ma, G. Y.; Khan, S. I.; Jacob, M. R.; Tekwani, B. L.; Li, Z. Q.; Pasco, D. S.; Walker, L. A.; Khan, I. A. *Antimicrob. Agents Chemother.* **2004**, *48* (11), 4450–4452.

(5) Hu, Y. Z.; An, J. Y.; Jiang, L. J. *J. Photochem. Photobiol., B* **1993**, *17*, 195–201.

(6) He, Y. Y.; An, J. Y.; Jiang, L. J. *Tetrahedron Lett.* **1998**, *39*, 5069–5072.

(7) Ou, Z. Z.; Chen, J. R.; Wang, X. S.; Zhang, B. W.; Cao, Y. *New J. Chem.* **2002**, *26*, 1130–1136.

(8) Qiao, R.; Zeng, Z. H.; Xia, S. Q.; Zhou, J. H.; Liu, Y. Y.; Chen, J. R.; Wang, X. S.; Zhang, B. W. *New J. Chem.* **2007**, *31*, 196–198.

(9) (a) Zeng, Z. H.; Qiao, R.; Zhou, J. H.; Xia, S. Q.; Zhang, Y.; Liu, Y. Y.; Chen, J. Q.; Wang, X. S.; Zhang, B. W. *J. Phys. Chem. B* **2007**, *111*, 3742–3749. (b) Xia, S. Q.; Zhou, J. H.; Chen, J. R.; Wang, X. S.; Zhang, B. W. *Chem. Commun.* **2003**, 2900–2901.

(10) (a) Zeng, Z. H.; Zhou, J. H.; Zhang, Y.; Qiao, R.; Xia, S. Q.; Chen, J. R.; Wang, X. S.; Zhang, B. W. *J. Phys. Chem. B* **2007**, *111*, 2688–2696. (b) Zhou, J. H.; Liu, J. H.; Xia, S. Q.; Wang, X. S.; Zhang, B. W. *J. Phys. Chem. B* **2005**, *109*, 19529–19535. (c) Zhou, J. H.; Xia, S. Q.; Chen, J. R.; Wang, X. S.; Zhang, B. W. *Chem. Commun.* **2003**, 1372–1373. (d) Ma, J. H.; Zhao, J. Q.; Jiang, L. J. *New J. Chem.* **2001**, *25*, 847–852. (e) Hu, Y. Z.; An, J. Y.; Jiang, L. J. *J. Photochem. Photobiol. B* **1994**, *22*, 219–227. (f) Diwu, S. J.; Zhang, C. L.; Lown, J. W. *J. Photochem. Photobiol. A* **1992**, *66*, 99–112.

 Published on Web 09/27/2010

Scheme 1. Molecular Structures of the Complexes Investigated

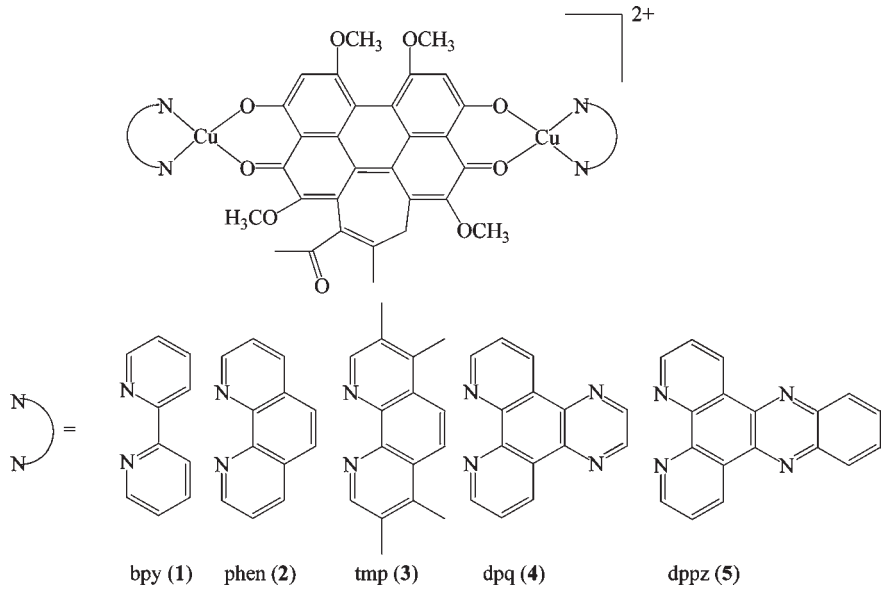

complexes exhibit larger binding affinity toward double-stranded DNA (dsDNA), one of the potential biotargets of PDT agents. However, because of the presence of two metal ion chelating sites in the structures of HA and HB, polymeric metal ion complexes without definite molecular formula and molecular weight were generally obtained,[10] which do not meet the criteria of single component for an ideal PDT agent. Additionally, the metal ions examined so far for this purpose, such as Al^{3+} and rare earth trivalent ions are all redox-inactive. Except for a few cases in which the metal ion complexes of hypocrellins show enhanced generation efficiency of singlet oxygen ($^1O_2$), the reactive oxygen species (ROS) contributing to the PDT activity of type II mechanism, most metal ion complexes suffer from decreased $^1O_2$ quantum yields compared to the natural hypocrellins.[10] The chelation of hypocrellins to the metal ions that possess biologically accessible redox potentials is expected to favor electron transfer processes and therefore may facilitate the formation of superoxide anion radical ($O_2^{-\bullet}$) or hydroxyl radical (•OH), the ROS responsible for the PDT activity of type I mechanism. Thus, we designed and synthesized a series of new dinuclear Cu(II) complexes (Scheme 1) with definite molecular formula, using HB as bridging ligand and diimine ligand as terminal ligand. The rationale for the choice of Cu^{2+} as the central metal ion is that it has an important biological role in all living organisms as an essential trace element and its Cu(II)−Cu(I) redox behavior is biologically available. More importantly, the redox-active feature renders many copper complexes remarkable DNA cleavage activities either in the presence of reducing or oxidizing additives (e.g., thiol compounds or hydrogen peroxide, the so-called chemical nuclease activity)[11] or upon irradiation of proper wavelength (the so-called photonuclease activity).[12] Five kinds of diimine ligands, including 2,2′-bipyridine (bpy), 1,10-phenanthroline (phen), 3,4,7,8-tetramethyl-1,10-phenanthroline (tmp), dipyrido[3,2-*f*:2′,3′-*h*]quinoxaline (dpq), and dipyrido-[3,2-*a*:2′,3′-*c*]phenazene (dppz), were utilized to finely modulate the photophysical and electrochemical properties as well as the binding affinities and the photocleavage activities toward dsDNA. As expected, the photonuclease activities of the Cu^{2+}-HB complexes are highly terminal ligand-dependent, and tmp-, dpq-, and dppz-based complexes (complex **3**, **4**, and **5**) exhibit much-improved photo nuclease activity than HB. Furthermore, the DNA photocleavage switches from a type II mechanism for HB to a type I mechanism for the Cu^{2+}-HB complexes, fully demonstrating the role of the redox-active Cu^{2+} ion.

2. Experimental Section

2.1. Materials. HB was isolated from fungus sacs of hypocrella bambusae and recrystallized three times from acetone before use. Ethidium bromide (EB), $Cu(OAc)_2 \cdot H_2O$, NH_4PF_6, superoxide dismutase (SOD), 1,4-diazabicyclo[2,2,2]octane (DABCO), 2,2,6,6-tetramethyl-4-piperidone (TEMP), 5,5-dimethyl-1-pyrroline-N-oxide (DMPO), 2,2′-bipyridine (bpy), 1,10-phenanthroline (phen), 3,4,7,8-tetramethyl-1,10-phenanthroline (tmp), *p*-benzoquinone (PBQ), calf thymus DNA (CT-DNA), gel loading buffer, and tris-hydroxymethyl-aminomethane (Tris base) were purchased from Sigma-Aldrich. The supercoiled pBR322 plasmid DNA was obtained from TaKaRa Biotechology Company. Dipyrido[3,2-*d*:2′,3′-*f*] quinoxaline (dpq) and dipyrido[3,2-*a*:2′,3′-*c*] phenazene (dppz) were synthesized following the reported methods.[13]

(11) (a) Arbuse, A.; Font, M.; Martinez, M. A.; Fontrodona, X.; Prieto, M. J.; Moreno, V.; Sala, X.; Llobet, A. *Inorg. Chem.* **2009**, *48*, 11098–11107. (b) Melvin, M. S.; Tomlinson, J. T.; Saluta, G. R.; Kucera, G. L.; Lindquist, N.; Manderville, R. A. *J. Am. Chem. Soc.* **2000**, *122*, 6333–6334. (c) Sigman, D. S.; Mazumder, A.; Perrin, D. M. *Chem. Rev.* **1993**, *93*, 2295–2316.

(12) (a) Sovan Roy, S.; Saha, S.; Majumdar, R.; Dighe, R. R.; Chakravarty, A. R. *Inorg. Chem.* **2009**, *48*, 9501–9509. (b) Maity, B.; Roy, Mithun.; Saha, S.; Chakravarty, A. R. *Organometallics* **2009**, *28*, 1495–1505. (c) Roy, M.; Pathak, B.; Patra, A. K.; Jemmis, E. D.; Nethaji, M.; Chakravarty, A. R. *Inorg. Chem.* **2007**, *46*, 11122–11132. (d) Dhar, S.; Nethaji, M.; Chakravarty, A. R. *Inorg. Chem.* **2006**, *45*, 11043–11050. (e) Brezova, V.; Valko, M.; Breza, M.; Morris, H.; Telser, J.; Dvoranova, D.; Kaiserova, K.; Varecka, L.; Mazur, M.; Leibfritz, D. *J. Phys. Chem. B* **2003**, *107*, 2415–2425. (f) Dhar, S.; Senapati, D.; Das, P. K.; Chattopadhyay, P; Nethaji, M.; Chakravarty, A. R. *J. Am. Chem. Soc.* **2003**, *125*, 12118–12124. (g) Dhar, S.; Senapati, D.; Reddy, P. D. N.; Das, P. K.; Chakravarty, A. R. *Chem. Commun.* **2003**, 2452–2453.

(13) (a) Collins, J. G.; Sleeman, A. D.; Aldrich-Wright, J. R.; Greguric, I.; Hambley, T. W. *Inorg. Chem.* **1998**, *37*, 3133–3141. (b) Amouyal, E.; Homsi, A.; Chambron, J. C.; Sauvage, J. P. *J. Chem. Soc., Dalton Trans.* **1990**, 1841–1845.

2.2. Synthesis. The five Cu^{2+}-HB complexes were prepared following a published method.[14] Taking $[Cu_2(HB)(bpy)_2](PF_6)_2$ (**1**) as an example, the procedures are as follows. 1.0 g of $Cu(OAc)_2.H_2O$ (5 mmol) dissolved in 50 mL of ethanol was mixed with a 50 mL of ethanol solution containing 0.78 g of bpy (5 mmol) and 2.0 g of NH_4PF_6 (12.3 mmol). Then, the mixture was dropped slowly into a 50 mL of CH_2Cl_2 solution of HB (1.32 g, 2.5 mmol). The solution was refluxed for 8 h under a N_2 atmosphere and filtered after cooling. The filtrate was subjected to dryness on a rotary evaporator, and the maroon solid was purified by column chromatography on silica gel using $CH_3CN/H_2O/KNO_3$ (50:5:1) as eluent. The product was further purified by recrystallization from CH_3CN-ethyl ether. The yield was 60%. The other complexes were prepared similarly by using the corresponding diimine ligands.

$[Cu_2(HB)(bpy)_2](PF_6)_2$ (1). ESI-MS: m/z = 483.0 (calcd value = 482.9 for $[Cu_2(HB)(bpy)_2]^{2+}$ ion). Anal. Calcd for $C_{50}H_{38}F_{12}N_4O_9P_2Cu_2 \cdot H_2O$: C, 47.14; H, 3.16; N, 4.40. Found: C, 47.04; H, 3.15; N, 4.26.

$[Cu_2(HB)(phen)_2](PF_6)_2$ (2). ESI-MS: m/z = 507.2 (calcd value = 507.0 for $[Cu_2(HB)(phen)_2]^{2+}$ ion). Anal. Calcd for $C_{54}H_{38}F_{12}N_4O_9P_2Cu_2 \cdot H_2O$: C, 49.06; H, 3.05; N, 4.24. Found: C, 49.37; H, 3.10; N, 3.99.

$[Cu_2(HB)(tmp)_2](PF_6)_2$ (3). ESI-MS: m/z = 563.3 (calcd value = 563.1 for $[Cu_2(HB)(tmp)_2]^{2+}$ ion). Anal. Calcd for $C_{62}H_{54}F_{12}N_4O_9P_2Cu_2 \cdot H_2O$: C, 52.25; H, 3.89; N, 3.93. Found: C, 52.55; H, 4.03; N, 3.85.

$[Cu_2(HB)(dpq)_2](PF_6)_2$ (4). ESI-MS: m/z = 559.2 (calcd value = 559.0 for $[Cu_2(HB)(dpq)_2]^{2+}$ ion). Anal. Calcd for $C_{58}H_{38}F_{12}N_4O_9P_2Cu_2 \cdot H_2O$: C, 48.85; H, 2.83; N, 7.86. Found: C, 48.58; H, 3.07; N, 7.92.

$[Cu_2(HB)(dppz)_2](PF_6)_2$ (5). ESI-MS: m/z = 608.9 (calcd value = 609.0 for $[Cu_2(HB)(dppz)_2]^{2+}$ ion). Anal. Calcd for $C_{66}H_{42}F_{12}N_4O_9P_2Cu_2 \cdot H_2O$: C, 51.94; H, 2.91; N, 7.34. Found: C, 52.07; H, 3.08; N, 7.36.

2.3. Spectroscopic Measurements. The mass spectra were determined on a Q-Tof Mass Spectrometry (Waters). The elemental analysis was performed on an Elementar Vario EL instrument.

The UV−vis absorption spectra and fluorescence emission spectra were recorded on a Shimadzu UV-1601PC spectrophotometer and a Hitachi F-4500 fluorescence spectrophotometer, respectively. The redox potentials were measured on an EG&G model 283 potentiostat/galvanostat in a three-electrode cell with a platinum-wire working electrode, a platinum-plate counter electrode, and a SCE (saturated calomel electrode) reference electrode. The cyclic voltammetry was conducted at a scan rate of 50 mV/s in a N_2-saturated, anhydrous dimethylformamide (DMF) solution containing 0.1 M tetra-n-butylammonium hexafluorophosphate as the supporting electrolyte.

The EPR spectra were taken at room temperature on a Bruker ESP-300E spectrometer at 9.8 GHz, X-band with 100 Hz field modulation. Samples were injected quantitatively into quartz capillaries and illuminated in the cavity of the EPR spectrometer with a Nd:YAG laser at 532 nm (5−6 ns of pulse width, 10 Hz of repetition frequency, 30 mJ/pulse energy).

2.4. Methods. All experiments involving CT-DNA were performed in PBS buffer solution (pH 7.4), unless otherwise noted. CT-DNA solutions were prepared by dispersing the desired amount of DNA in buffer solution with stirring overnight at temperature below 4 °C. The concentration of CT-DNA was expressed as the concentration of nucleotide and was calculated using the extinction coefficient of 6600 M^{-1} cm^{-1} at 260 nm.

2.4.1. Absorption Titration for DNA Binding. The DNA binding constants of the complexes were determined by monitoring the absorption spectrum changes of the complexes upon increasing the concentration of CT-DNA.[15] The binding constants (K_b) and the binding site sizes (s) were obtained by fitting the titration data to the eqs 1 and 2:

$$(\varepsilon_a - \varepsilon_f)/(\varepsilon_b - \varepsilon_f) = (b - (b^2 - 2K_b^2 C_t[\mathrm{DNA}]/s)^{1/2})/2K_b C_t \quad (1)$$

$$b = 1 + K_b C_t + K_b[\mathrm{DNA}]/2s \quad (2)$$

where ε_f and ε_b are the extinction coefficients at the absorption maximum of the free and bound complex, respectively. ε_a is the apparent extinction coefficient of the complex in the presence of CT-DNA. [DNA] denotes the concentration of CT-DNA in nuclear phosphate, whereas C_t is the concentration of the complex.

2.4.2. EB Displacement Assay for DNA Binding. To a 2 mL of solution of EB (5 μM) and CT-DNA (10 μM in base pair) in PBS buffer, aliquots of the complex solution (0.5 mM in CH_3CN) were added and kept standing for 15 min before fluorescence measurements (490 nm excitation). The apparent binding affinity K_{app} was calculated from the eq 3:

$$K_{EtBr}[\mathrm{EtBr}] = K_{app}[\mathrm{drug}] \quad (3)$$

where [drug] is the concentration of the copper complex at a 50% reduction of EB fluorescence and K_{EtBr} is the binding constant of EB toward CT-DNA (1×10^7 M^{-1}).[16]

2.4.3. DNA Viscosity Experiments. The viscosity measurements were carried out using a Ubbelodhe viscometer immersed in a constant temperature bath at 30 °C and a stopwatch. The data were presented as $(\eta/\eta_0)^{1/3}$ vs [complex]/[DNA], where η is the specific viscosity of DNA in the presence of complexes and η_0 is the specific viscosity of DNA alone in PBS buffer. Specific viscosity values were calculated from the observed flow time of DNA solutions (t) corrected for the buffer alone (t_0), $\eta = (t - t_0)/t_0$.[17]

2.4.4. Gel Electrophoresis for DNA Photocleavage. DNA photocleavage abilities of the complexes were evaluated using supercoiled pBR322 plasmid DNA as target. The mixture of 50 μL of supercoiled pBR322 DNA (30 μM in base pair) in PBS buffer and 10 μL of examined complex in CH_3CN (0.5 mM) was irradiated under a solar simulator, using a filter to cut off the light of < 550 nm. After irradiation, 15 μL of gel loading buffer was added. The sample was then subjected to agarose gel (1%) electrophoresis (Tris-acetic acid-EDTA buffer, pH 8.0) at 80 V for about 2 h. The gel was stained with 1 mg/L EB for 1 h, and then analyzed using Gel Doc XR system (Bio-Rad).

2.4.5. n-Octanol/Water Partition Coefficients. The n-octanol/water partition coefficients ($P_{o/w} = C_o/C_w$) were measured at room temperature following a reported method.[18] In brief, solutions of each complex (1 mM) in equal volumes of PBS (pH 7.4, 1 mL) and n-octanol (1 mL) were mixed and sonicated for 30 min. After separation by centrifugation, the amounts of complex in each phase were determined after dilution with DMF by absorbance intensity on a Shimadzu UV-1601PC spectrophotometer and the results were the average of three independent measurements.

3. Results and Discussion

3.1. Synthesis and Water Solubility. The reflux of the ethanol/CH_2Cl_2 solution of $Cu(OAc)_2$, diimine ligand,

(14) (a) Katsarou, M. E.; Efthimiadou, E. K.; Psomas, G.; Karaliota, A.; Vourloumis, D. *J. Med. Chem.* **2008**, *51*, 470–478. (b) Merrell, P. H. *Inorg. Chim. Acta* **1979**, *32*, 99–102.

(15) (a) Nair, R. B.; Teng, E, S.; Kirkland, S. L.; Murphy, C. J. *Inorg. Chem.* **1998**, *37*, 139–141. (b) Carter, M. T.; Rodriguez, M.; Bard, A. J. *J. Am. Chem. Soc.* **1989**, *111*, 8901–8911.

(16) Lee, M.; Rhodes, A. L.; Wyatt, M. D.; Forrow, S.; Hartley, J. A. *Biochemistry* **1993**, *32*, 4237–4245.

(17) Cohen, G.; Eisenberg, H. *Biopolymers* **1969**, *8*, 45–55.

(18) Kepczynski, M.; Pandian, R. P.; Smith, K. M.; Ehrenberg, B. *Photochem. Photobiol.* **2002**, *76*, 127–134.

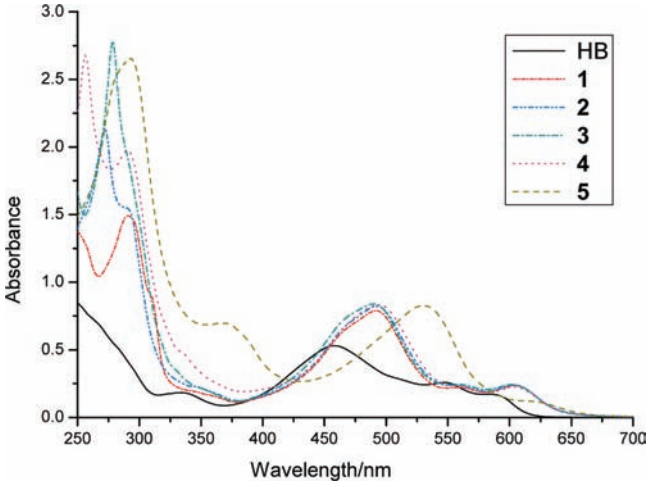

Figure 1. Electronic absorption spectra of complex **1**−**5** and HB in acetonitrile (20 μM).

and HB in a stoichiometric ratio of 2:2:1 gave the target complexes in high yields. The hexafluorophosphate salts of the five complexes were recrystallized from CH_3CN-ethyl ether as maroon solid, and their chemical identities were confirmed by both mass spectra (see Figure S1−S5 in the Supporting Information) and elemental analysis. We failed to obtain the crystals of these complexes that are suitable for X-ray diffraction analysis. We measured the powder EPR spectra of these complexes at room temperature and at 77K (see Figure S6 in the Supporting Information). Though no fine structures can be resolved even at 77K, and thus no detailed structural information can be deduced, the EPR spectra indeed provide the evidence of Cu(II) oxidation state. The solution EPR spectra of the complexes in DMF or in CH_3CN are nearly the same as the powder EPR spectra, except having lower intensities. Similar EPR spectra were also found in other dinuclear Cu(II) complexes.[19]

All the complexes are soluble in acetonitrile, acetone, and DMF/PBS buffer mixed solution (1:9 in volume ratio). The n-octanol/water partition coefficients $P_{o/w}$ ($= C_o/C_w$) of the complexes were measured to be 0.48 for **1**, 0.17 for **2**, 0.18 for **3**, 0.73 for **4**, and 1.50 for **5**, whereas that of HB is as high as 42.24, indicating much-improved water solubility for the Cu^{2+}-HB complexes.

3.2. Photophysical Properties. Figure 1 shows the absorption spectra of HB and the five Cu^{2+}-HB complexes in acetonitrile. HB has three absorption bands in the visible region centered at 450 nm (named A band for the following discussion), 535 and 584 nm, respectively. Similar to the other metal ion complexes of HB,[10] the coordination of Cu^{2+} ions leads to significant red shift of the three absorption bands (Table 1). As a result, the absorption onsets of the five complexes extend to ca. 675 nm, compared to that of 625 nm for HB, favoring their application in PDT.

Accompanying the red shift, the A band also undergoes a remarkable increase in absorbance. Additionally, for **5**, the A band red shifts to 530 nm, in sharp contrast to about 490 nm for the other four complexes. Generally, the A band is assigned to the $\pi-\pi^*$ transition of the conjugated system consisting of the quinone carbonyl group and the perylene nucleus.[20] The phenomena we observed hint somewhat charge transfer (CT) character of the A band. The Cu^{2+} coordination to the carbonyl group may promote the CT process, therefore shifts the absorption maximum of the A band to longer wavelength and increases the absorbance at the same time. The quite different photophysical property of complex **5** from the other four complexes likely stems from the unique π-delocalization character of the dppz ligand. It is well-known that $[Ru(II)(bpy)_2(dppz)]^{2+}$ possesses two MLCT excited states on the dppz ligand, a luminescent state associated with the bpy fragment and a lower-lying but nonluminescent state localized largely on the phenazine (phz) portion.[21] Such a lower-lying phz-associated charge transfer state might be also present in complex **5**, which may interact with the excited state responsible for the A band and lead to the dramatic red shift of the A band.

Cu(II) complexes generally exhibit a broad but very weak copper-centered d−d transition band in the region of 500−800 nm.[12f,g] For the Cu^{2+}-HB complexes, the d−d band is most likely buried in the strong visible absorption bands of the HB chromophore. The absorption of the Cu^{2+}-HB complexes in the UV region is dominated by the diimine ligands.

While HB is fluorescent,[20] no fluorescence emission was detected upon illumination of the Cu^{2+}-HB complexes, regardless of the excitation wavelength. The fluorescence quenching of HB upon coordination of Cu^{2+} ions may be associated with the paramagnetic character of Cu^{2+} or originate from the energy or electron transfer from HB to Cu^{2+}.[22,23]

We also examined the photochemical stability of the Cu^{2+}-HB complexes. Upon irradiation with the light of $\geq$550 nm for 45 min (a condition similar to the DNA photocleavage experiments), the absorption spectra of the Cu^{2+}-HB complexes in DMF/(Tris-CH_3COOH/EDTA buffer) (pH 7.4) solutions did not show any changes (see Figure S7 in the Supporting Information), suggesting a satisfactory photochemical stability.

3.3. Electrochemical Properties. The electrochemical properties of complex **1**−**5** and HB in DMF were studied by cyclic voltammetry. HB exhibits two reversible redox processes attributed to $HB/HB^{-\cdot}$ and $HB^{-\cdot}/HB^{2-}$, with half wave potentials of −0.33 V and −0.65 V vs SCE, respectively (see Figure S8a in the Supporting Information). For complex **1**, the two HB-based redox processes can also be found in the potential range of −0.3 to −0.8 V, but no longer reversible (see Figure S8b in the Supporting Information). A new redox process was found in the potential range of 0−0.5 V. This new redox process is electrochemically irreversible, and the voltammgram profiles are highly

(19) (a) Padmanabhan, M.; Meena Kumary, S.; Huang, X.; Li, J. *Inorg. Chim. Acta* **2005**, *358*, 3537–3544. (b) Voronkova, V.; Galeev, R.; Korobchenko, L.; Madalan, A. M.; Andruh, M.; Kravtsov, V. C.; Simonov, Y. A. *Appl. Magn. Reson.* **2005**, *28*, 297–310.

(20) Diwu, Z. J.; Jiang, L. J.; Zhang, M. H. *Sci. China, Ser. B: Chem.* **1990**, *33*, 18–26.

(21) (a) Brennaman, M. K.; Meyer, T. J.; Papanikolas, J. M. *J. Phys. Chem. A* **2004**, *108*, 9938–9944. (b) Brennaman, M. K.; Alstrum-Acevedo, J. H.; Fleming, C. N.; Jang, P.; Meyer, T. J.; Papanikolas, J. M. *J. Am. Chem. Soc.* **2002**, *124*, 15094–15098.

(22) Volchkov, V. V.; Ivanov, V. L.; Uzhinov, B. M. *J. Fluoresc.* **2010**, *20*, 299–303.

(23) (a) Varnes, A. W.; Dodson, R. B.; Wehry, E. L. *J. Am. Chem. Soc.* **1972**, *94*, 946–950. (b) Kemlo, J. A.; Shepherd, T. M. *Chem. Phys. Lett.* **1977**, *47*, 158–162.

Table 1. Selected Physicochemical Data and DNA Binding Properties of Complex **1**−**5**

complex	absorption maximum $\lambda_{max/nm}$ (ε (M^{-1} cm^{-1}))[a]	E_p (V) (vs SCE)[b]	E'_p (V) (vs SCE)[c]	K_b ($\times 10^5$ M^{-1}) (s)[d]	$K_{app} \times 10^5$ M^{-1}[e]
HB	455 (26350), 548 (12900), 588 (8450)		1.07, 1.28	0.86 (0.10)	3.24
$[Cu_2(HB)(bpy)_2](PF_6)_2$ (**1**)	490 (39300), 562 (11000), 603 (11850)	0.16, 0.27	1.07, 1.29	3.90 (0.12)	5.41
$[Cu_2(HB)(phen)_2](PF_6)_2$(**2**)	491 (41000), 562 (11550), 603 (11900)	0.22, 0.32	1.09, 1.34	4.20 (0.42)	7.77
$[Cu_2(HB)(tmp)_2](PF_6)_2$ (**3**)	492 (41850), 563 (12000), 603 (12100)	0.13, 0.28	1.09, 1.31	9.17 (0.21)	13.90
$[Cu_2(HB)(dpq)_2](PF_6)_2$ (**4**)	492 (41650), 563 (11450), 603 (11250)	0.19, 0.27	1.09, 1.31	5.39 (0.18)	9.65
$[Cu_2(HB)(dppz)_2](PF_6)_2$ (**5**)	530 (41350), 623 (5700)	0.22, 0.34	1.10, 1.31	6.00 (0.19)	10.40

[a] In acetonitrile. [b] Peak potentials for irreversible Cu(II)−Cu(I) couple in DMF. [c] Peak potentials for irreversible oxidation of HB moiety in DMF. [d] Obtained by absorption titration. [e] Obtained by EB displacement assay.

dependent on the potential scan range (see Figure S8b−f in the Supporting Information). In proper scan condition, the redox process exists in a double-peak manner. Similar results were also observed in the cases of complexes **2**−**5**. We tentatively ascribe the double peaks to the Cu(II,II)/Cu(II, I) and Cu(II, I)/Cu(I,I) couples, and the peak potentials are listed in Table 1. Many Cu(II) complexes possess similar Cu(II)/Cu(I) potentials, supporting our assignment.[12,24]

3.4. DNA Binding. DNA binding plays an important role for a DNA cleaver. In our work, absorption titration was employed to compare the binding capabilities of the Cu^{2+}-HB complexes toward CT-DNA. Upon addition of CT-DNA into the solutions of the complexes, the absorption bands belonging to the HB chromophore underwent a significant absorbance decrease, i.e., the hypochromism. As an example, Figure 3a shows the case of complex **4** (also see Figure S9 in the Supporting Information). The hypochromism effect suggests an intercalation binding mode of the complexes with CT-DNA, and the HB moiety acts as the intercalating body. Though the Cu^{2+}-HB complexes and HB bind CT-DNA by the same intercalation mode, there are great differences in their binding affinities. The binding constants (Table 1) of the Cu^{2+}-HB complexes fall in the range of $3.90-9.17 \times 10^5$ M^{-1}, much higher than that of HB (0.86×10^5 M^{-1}). Clearly, the electrostatic attraction between the cationic Cu^{2+}-HB complexes and the negatively charged dsDNA play a positive role. The influences of the terminal diimine ligands are also remarkable on the binding. The binding constants of the Cu^{2+}-HB complexes follow the order **3** (tmp) > **5** (dppz) > **4** (dpq) > **2** (phen) > **1** (bpy). The highest binding constant of **3** most likely results from the strong hydrophobic interaction between the methyl groups of tmp ligand and the hydrophobic interior accessible in DNA.[25] The higher binding constants of **5** and **4** than that of **2** and **1** may be either due to the higher intercalation propensity of dppz and dpq ligands than phen and bpy ligands or due to the higher hydrophobic feature of **5** and **4** than **2** and **1**. Interestingly, the binding to CT-DNA also leads to an absorption spectrum red shift for complexes **1**, **2**, and **3**. In contrast, only hypochromism effect was observed in the cases of HB, complex **4** and **5**. This finding reminds us further the subtle effects of the terminal diimine ligands on binding.

We also used EB displacement assay to determine the apparent binding constants (K_{app}) of the Cu^{2+}-HB complexes to CT-DNA. EB itself is weakly emissive, but exhibits strong fluorescence emission when bound to DNA. The addition of the Cu^{2+}-HB complexes into the EB-CT-DNA solution led to the quenching of the EB fluorescence (Figure 2b shows the case of **3**, also see Figure S10 in the Supporting Information). In the absence of CT-DNA, the influence of the Cu^{2+}-HB complexes is negligible on the fluorescence intensity of EB. Thus, the fluorescence quenching may be attributed to the competitive binding of the Cu^{2+}-HB complexes to CT-DNA. The binding constants measured in this way (Table 1) indicate further that the Cu^{2+}-HB complexes bind DNA more effectively than the parent HB. Moreover, the apparent binding constants (K_{app}) follow the order **3** (tmp) > **5** (dppz) > **4** (dpq) > **2** (phen) > **1** (bpy), in good agreement with the results obtained from the absorption titration.

To better understand the nature of the DNA binding, we carried out specific viscosity measurements of CT-DNA in the presence of varied concentrations of the Cu^{2+}-HB complexes. As shown in Figure 3, with the gradual addition of the Cu^{2+}-HB complexes or HB, the specific viscosity of CT-DNA increased linearly. The marked viscosity increase in CT-DNA is indicative of an intercalation interaction, resulting from the elongation of DNA helix caused by the insertion of planar aromatic chromophores between base pairs.[26] The largest viscosity increase of CT-DNA occurred in the case of **5**, suggesting an involvement of dppz in binding due to its strong intercalating capability. Though a $[Ru(phen)_2dppz]^{2+}$ dimer with a flexible aliphatic diamide linker was confirmed to reach its bis-intercalated binding geometry via threading,[27] Turro group has shown that $[(bpy)_2Ru(tpphz)Ru(bpy)_2]^{4+}$ cannot bind dsDNA in a threading fashion.[28] Because of the structure similarity between complex **1**-**5** and $[(bpy)_2Ru(tpphz)Ru(bpy)_2]^{4+}$, the most likely binding mode is the "partial" intercalation of HB moiety from the bay region. In case of **5**, the "full" intercalation via dppz terminal may compete with that via HB moiety. This may explain why **5** enhanced the DNA specific viscosity most efficiently, though its apparent binding constant is not the largest one.

3.5. Chemical Nuclease Activity. Many Cu(II) complexes show chemical nuclease activity in the presence of a reducing agent such as ascorbic acid or 3-mercaptopropionic

(24) Barve, A.; Kumbhar, A.; Bhat, M.; Joshi, B.; Butcher, R.; Sonawane, U.; Joshi, R. *Inorg. Chem.* **2009**, *48*, 9120–9132.
(25) (a) Ramakrishnan, S.; Rajendiran, V.; Palaniandavar, M.; Periasamy, V. S.; Srinag, B. S.; Krishnamurthy, H.; Akbarsha, M. A. *Inorg. Chem.* **2009**, *48*, 1309–1322. (b) Rajendiran, V.; Karthik, R.; Palaniandavar, M.; Stoeckli-Evans, H.; Periasamy, V. S.; Akbarsha, M. A.; Srinag, B. S.; Krishnamurthy, H. *Inorg. Chem.* **2007**, *46*, 8208–8221. (c) Chan, H. L.; Liu, H. Q.; Tzeng, B. C.; You, Y. S.; Peng, S. M.; Yang, M.; Che, C. M. *Inorg. Chem.* **2002**, *41*, 3161–3171.
(26) (a) Mahadevan, S.; Palaniandavar, M. *Inorg. Chem.* **1998**, *37*, 3927–3934. (b) Mahadevan, S.; Palaniandavar, M. *Inorg. Chem.* **1998**, *37*, 693–700.
(27) Önfelt, B.; Lincoln, P.; Nordén, B. *J. Am. Chem. Soc.* **1999**, *121*, 10846–10847.
(28) Lutterman, D. A.; Chouai, A.; Liu, Y.; Sun, Y.; Stewart, C. D.; Dunbar, K. R.; Turro, C. *J. Am. Chem. Soc.* **2008**, *130*, 1163–1170.

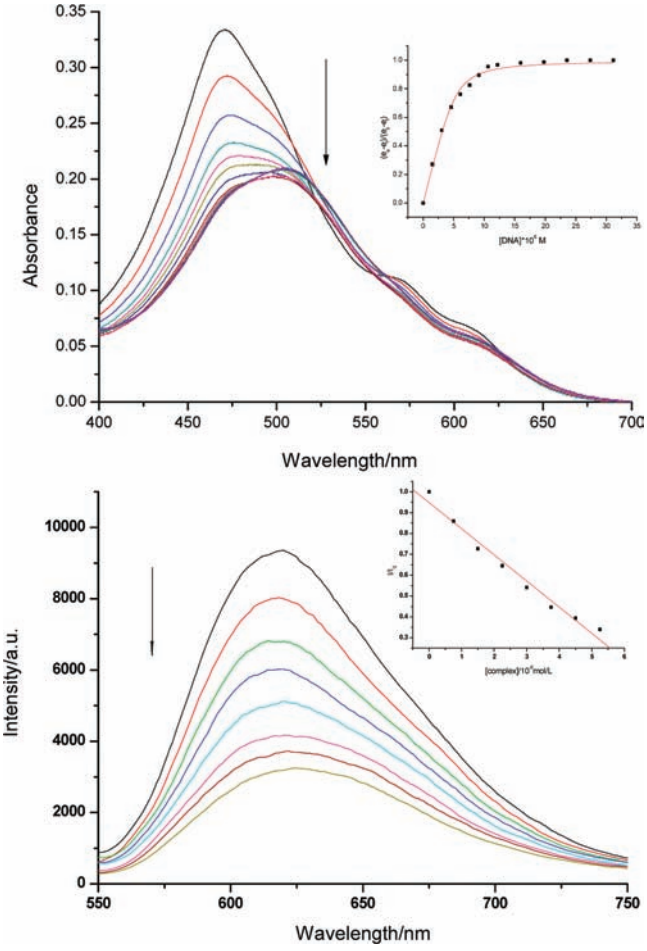

Figure 2. (a) Absorption spectra of complex **3** (2×10^{-4} M) in PBS buffer (pH 7.4) in the presence of varied concentrations of CT-DNA (from 0 μM to 31.16 μM). The inset shows the plot of $(\varepsilon_a - \varepsilon_f)/(\varepsilon_b - \varepsilon_f)$ vs [DNA]. (b) Fluorescence quenching of EB (5 μM) bound to CT-DNA (10 μM) by complex **3** (from 0 μM to 5.25 μM). Inset is the plot of I/I_0 vs [complex]. $\lambda_{e\,x}$ = 510 nm.

acid.[29] The chemical nuclease activities of the Cu^{2+}-HB complexes in the presence of ascorbic acid were studied by gel electrophoresis using supercoiled pBR322 plasmid DNA as target, Figure 4. Upon exposure to a solution containing both Cu^{2+}-HB complex and ascorbic acid for 1 h, supercoiled pBR322 plasmid DNA underwent remarkable DNA cleavage from the supercoiled form (Form I) to the nicked circular form (form II). Control experiments revealed that Cu^{2+}-HB or ascorbic acid alone cannot lead to DNA cleavage. Moreover, even in the presence of ascorbic acid, HB, bpy, phen, tmp, dpq, and dppz did not cleave DNA, whereas $Cu(OAc)_2$ showed a very weak nuclease activity. The higher chemical nuclease activities of **3**−**5** than **1** and **2** presumably result from their larger binding constants toward DNA (Table 1).

The mechanism of the chemical nuclease activity of complex **1**−**5** was investigated using various additives (Figure 5 and Figure S11 in the Supporting Information). The addition of NaN_3, the scavenger of singlet oxygen ($^1O_2$), has no any effect on DNA cleavage. The DNA cleavage restriction caused by superoxide dismutase

(29) (a) Patra, A. K.; Nethaji, M.; Chakravarty, A. R. *Dalton Trans.* **2005**, 2798–2804. (b) Patra, A. K.; Dhar, S.; Nethaji, M.; Chakravarty, A. R. *Dalton Trans.* **2005**, 896–902.

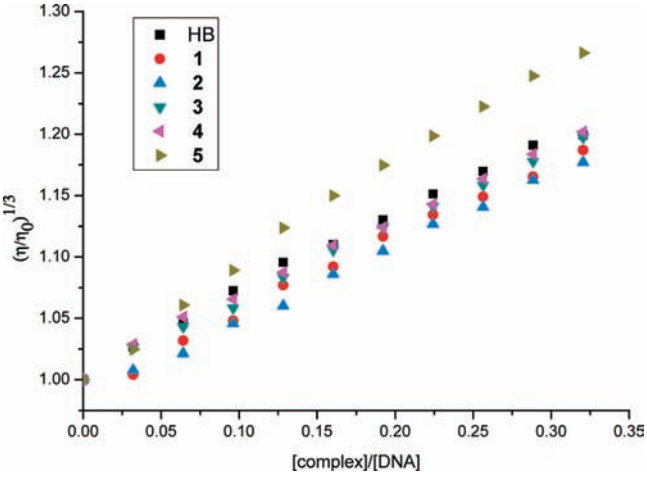

Figure 3. Relative specific viscosities of CT-DNA at 30.0 °C in 5 mM Tris-HCl buffer (pH 7.2) as the function of the concentration ratio of photosensitizer and CT-DNA ([DNA] = 130 μM, [photosensitizer] = 0−80 μM).

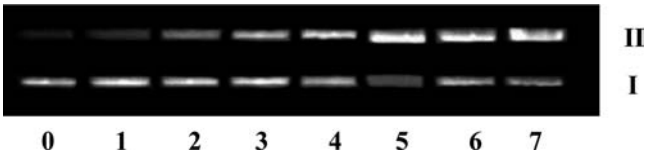

Figure 4. Agarose gel electrophoresis pattern of supercoiled pBR322 DNA after incubation with complex **1**−**5** in the presence of ascorbic acid (A) in Tris-CH_3COOH/EDTA buffer (pH 7.4) at 37 °C for 1 h. Lane 0, DNA alone; lane 1, DNA + A; lane 2, DNA + $Cu(OAc)_2 \cdot 4H_2O$ + A; lane 3, DNA + **1** + A; lane 4, DNA + **2** + A; lane 5, DNA + **3** + A; lane 6, DNA + **4** + A; lane 7, DNA + **5** + A. [DNA] = 30 μM, [complex] = 80 μM, [A] = 2.5 mM. Form I and II represent supercoiled circular and nicked circular forms, respectively.

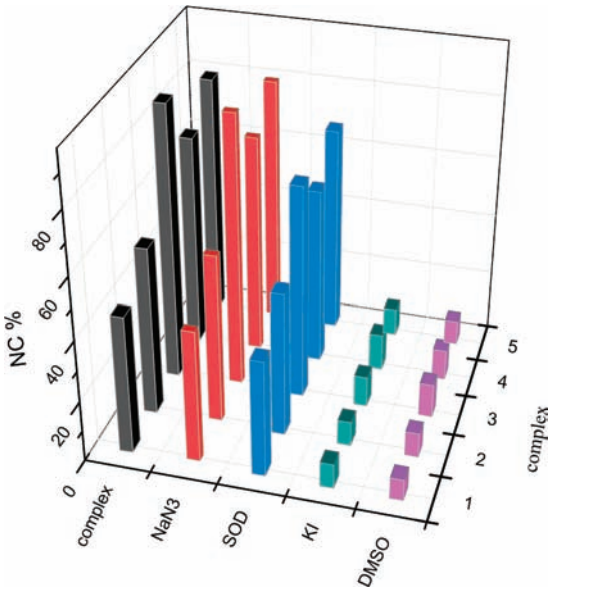

Figure 5. Histogram showing the influences of various additives on the chemical nuclease activities of complex **1-5** in the presence of ascorbic acid. [pBR 322 DNA] = 30 μM, [complex] = 80 μM, [ascorbic acid] = 2.5 mM, [NaN_3] = 50 mM, [SOD] = 1000 U/mL, [KI] = 50 mM.

(SOD), the scavenger of superoxide anion radical ($O_2^{-\bullet}$), is also negligible. However, the presence of DMSO or KI, the scavengers of hydroxyl radical (•OH), inhibits the

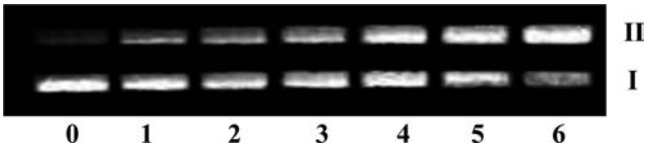

Figure 6. Agarose gel electrophoresis pattern of supercoiled pBR322 DNA in the presence of **1**−**5** upon visible irradiation (≥550 nm) for 45 min in air-saturated Tris-CH_3COOH/EDTA buffer (pH 7.4). Lane 0, DNA alone; lane 1, DNA + HB; lane 2, DNA + **1**; lane 3, DNA + **2**; lane 4, DNA + **3**; lane 5, DNA + **4**; lane 6, DNA + **5**. [DNA] = 30 μM, [complex] = 80 μM. Form I and II represent supercoiled circular and nicked circular forms, respectively.

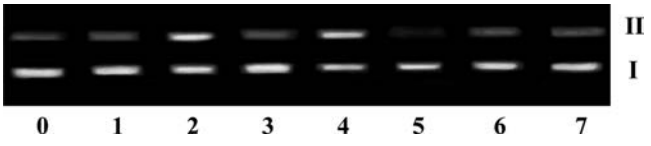

Figure 7. Agarose gel electrophoresis pattern of supercoiled pBR322 DNA in the presence of **5** upon visible irradiation (≥550 nm) for 40 min in air-saturated Tris-CH_3COOH/EDTA buffer (pH 7.4). Lane 0, DNA alone; lane 1, DNA + **5** (in dark); lane 2, DNA + **5**; lane 3, DNA + **5** (N_2); lane 4, DNA + **5** + DABCO; lane 5, DNA + **5** + PBQ; lane 6, DNA + **5** + KI; lane 7, DNA + **5** + DMSO. [DNA] = 30 μM, [**5**] = 80 μM, [DABCO] = [KI] = [PBQ] = 50 mM. Form I and II represent supercoiled circular and nicked circular forms, respectively.

DNA cleavage significantly, indicating that •OH is the main ROS responsible for the chemical nuclease activities of the Cu^{2+}-HB complexes. Many Cu(II) complexes cleave DNA by the same mechanism. It is generally believed that the reduction of Cu(II) to Cu(I) by reducing agent is the initial process, the resulting Cu(I) center then activates oxygen to form the hydroxyl radical.[29] The biologically available Cu(II)/Cu(I) potentials of the Cu^{2+}-HB complexes are obviously necessary for their chemical nuclease activities.

3.6. Photo Nuclease Activity. The DNA photocleavage activities of complex **1**−**5** were examined by the agarose gel electrophoresis pattern of supercoiled pBR322 DNA upon irradiation with visible light (≥550 nm) in air-saturated buffer. As shown in Figure 6, all the Cu^{2+}-HB complexes cleaved DNA upon visible irradiation, and the photo nuclease activities of complexes **3**−**5** are much higher than that of HB, which may be attributed to the enhanced binding affinity and ROS generation efficiency. When irradiation was carried out by the light ≥470 nm or ≥500 nm, shorter irradiation time (20 or 30 min) resulted in similar or larger extent of DNA cleavage than the case of 45 min irradiation by 550 nm (see Figures S12 and S13 in the Supporting Information). Further irradiation may lead to complete disappearance of Form I, but no Form III, i.e., the linear form of pBR322 DNA, was observed.

To explore the DNA photocleavage mechanisms of **1**−**5**, control experiments were carried out. **1**−**5** alone cannot cleave DNA in dark, indicating that the observed DNA cleavage originates from the excited complex. If the irradiation was performed in a N_2-saturated solution, all the complexes lost their photo nuclease activity (Figure 7, lane 3, taking **5** as an example), implying the involvement of molecular oxygen. In the presence of singlet oxygen quencher DABCO, marginal inhibition effect was observed (Figure 7, lane 4). However, the presence of hydroxyl radical scavengers DMSO and KI or superoxide anion radical scavenger *p*-benzoquinone (PBQ) inhibited DNA photocleavage remarkably (Figure 7, lane 5−7), demonstrating the key role of •OH and $O_2^{-\bullet}$. Figure S14 in the Supporting Information shows the case of complex **3**. The control experiments suggest a type I mechanism for the Cu^{2+}-HB complexes, in contrast to the type II mechanism for HB.[10]

Preliminary assessments were carried out for the cytotoxicity and phototoxicity of the complexes toward HepG2 cells, see Figure S15 in the Supporting Information. At the concentration of 1 μM, complexes **1**−**5** led to >90% of cell death upon 30 min of irradiation (>550 nm), whereas the percentage of cell death was only 40% in the absence of irradiation, indicating the photodynamic activities of these complexes. Though the nonemissive characters of the complexes hinder the direct observation of their cell uptake and subcellular localization, the cytotoxicity and phototoxicity suggest that these complexes may either bind on or penetrate through the cell membrane.

3.7. Generation of Superoxide Anion Radical and Hydroxyl Radical. Spin trapping is a powerful technique to detect the formation of reactive radical species. In our study, DMPO was used to trap $O_2^{-\cdot}$, and the obtained DMPO-$O_2^{-\cdot}$ adduct was monitored by EPR. Upon irradiation of air-saturated DMSO solution of complex **4** (1 mM) and DMPO (50 mM) with 532 nm laser, an EPR spectrum with hyperfine coupling constants of α^N = 13.0 G, α_β^H = 10.1 G, and α_γ^H = 1.5 G was observed (Figure 8, inset), attributable to DMPO-$O_2^{-\bullet}$.[30] Control experiments ensure that O_2, light, DMPO, and complex are all necessary for the EPR signal. The assignment was further confirmed by the quenching of the signal by SOD. The other Cu^{2+}-HB complexes showed similar behaviors as **4.** Figure 8 shows the DMPO-$O_2^{-\bullet}$ EPR signal intensities of the complexes at varied irradiation time (normalized to unity absorbance at 532 nm), and the $O_2^{-\bullet}$ generation abilities follow the order of **4** > **2** > **1** > **3** > HB > **5.**

The lower DMPO-$O_2^{-\bullet}$ signal intensity of **5** than HB is unexpected. Further experiments suggest that **5** can react with DMPO-$O_2^{-\bullet}$. Upon irradiation of air-saturated DMSO solution of **4** and DMPO with 532 nm laser, an EPR signal of DMPO-$O_2^{-\bullet}$ was obtained (Figure 9a). Then, 50 μL DMSO solution of **5** was added into the irradiated solution, a remarkable quenching of the DMPO-$O_2^{-\cdot}$ signal was observed (Figure 9d). The addition of 50 μL of DMSO or DMSO solution of the other Cu^{2+}-HB complexes did not influence EPR signal intensity (Figure 9b, c). Though the reaction mechanism between **5** and DMPO-$O_2^{-\cdot}$ is still unknown, the fact that the photo nuclease activity of **5** can be restricted dramatically by PBQ (Figure 7) suggests **5**, like its analogues **1**−**4**, may far exceed HB in $O_2^{-\bullet\cdot}$ generation.

HB and its Cu^{2+} complexes can generate $O_2^{-\bullet}$ upon irradiation; however, the underlying mechanisms may be greatly different. For HB, the formation of $O_2^{-\bullet}$ is believed to originate from the electron transfer from $HB^{-\bullet}$ to O_2, and $HB^{-\bullet}$ comes from the self-electron transfer between an excited HB and a ground-state HB (eqs 4 and 5).[31] In the cases of the Cu^{2+}-HB complexes, $O_2^{-\bullet}$ results most likely

(30) Harbour, J. R.; Hair, M. L. *J. Phys. Chem.* **1978**, *82*, 1397–1399.
(31) Liu, Y. Y.; Zhou, Q. X.; Zeng, Z. H.; Qiao, R.; Wang, X. S.; Zhang, B. W. *J. Phys. Chem. B* **2008**, *112*, 9959–9965.

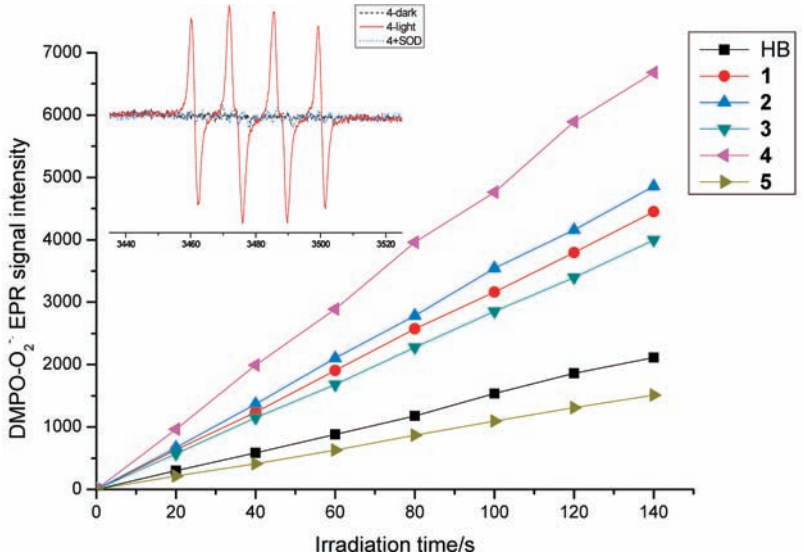

Figure 8. EPR signal intensity of DMPO−$O_2^{-\bullet}$ as the function of irradiation time. The inset shows the EPR spectrum of DMPO-$O_2^{-\bullet}$ obtained upon irradiation of air-saturated DMSO solution of complex **4** (1 mM) and DMPO (50 mM) with 532 nm laser.

from the activation of O_2 by Cu(I) species, which in turn is the product of the intramolecular electron transfer from the excited HB moiety to Cu(II) center (eqs 6 and 7), because of the high redox potential of Cu(II)/Cu(I) couple (Table 1).[12e] Taking complex **1** as an example, the first oxidation potential of the HB moiety is 1.07 eV vs SCE (Table 1), thus the singlet and triplet excited state oxidation potentials of −0.95 and −0.81 eV for the HB moiety can be roughly estimated by subtracting the singlet or triplet excited state energy of the HB moiety (199.58 and 180.75 kJ/mol [32]). Considering the reduction potentials of Cu(II) centers are in the range of 0.16−0.34 eV vs SCE, the electron transfer from the excited HB moiety (either singlet or triplet excited state) to the Cu(II) center, i.e., eq 6, is highly favorable in thermodynamics.

$$HB^{*} + HB \rightarrow HB^{+\bullet} + HB^{-\bullet} \quad (4)$$

$$HB^{-\bullet} + O_2 \rightarrow HB + O_2^{-\bullet} \quad (5)$$

$$Cu^{2+} - HB \rightarrow Cu^{2+} - HB^{*} \rightarrow Cu^{+} - HB^{+\bullet} \quad (6)$$

$$Cu^{+} - HB^{+\bullet} + O_2 \rightarrow Cu^{2+} - HB^{+\bullet} + O_2^{-\bullet} \quad (7)$$

Upon irradiation of air-saturated CH_3CN-H_2O (9:1 in volume ratio) solution of complex **4** (1 mM) and DMPO (50 mM) with 532 nm laser, a four-line EPR spectrum with the intensity ratio of 1:2:2:1 and hyperfine coupling constants of $\alpha^N = \alpha^H = 14.9$ G was observed, which may be assigned to DMPO−OH adduct signal (Figure 10, inset).[33] Control experiments ensure that O_2, light, DMPO, and complex are all necessary for the EPR signal. The assignment was further confirmed by the quenching of the signal by KI. Other complexes showed similar

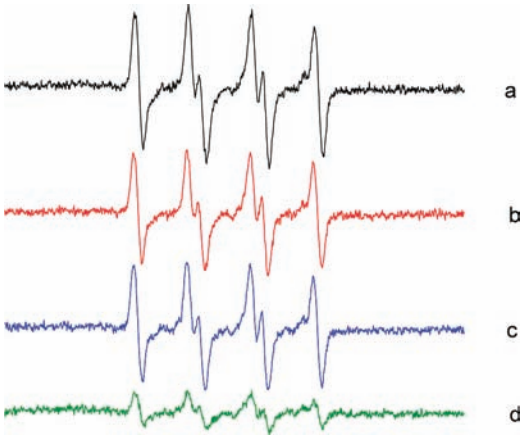

Figure 9. EPR spectra obtained, respectively, (a) upon irradiation (at 532 nm) of an air-saturated DMSO solution containing 50 mM DMPO and 1 mM complex **4**; (b) upon addition of 50 μL DMSO into the irradiated solution; (c) upon addition of 50 μL DMSO solution of complex **2** (1 mM) into the irradiated solution; (d) upon addition of 50 μL DMSO solution of complex **5** (1 mM) into the irradiated solution.

behaviors as complex **4.** Figure 10 shows the DMPO−OH EPR signal intensities of the complexes at varied irradiation time (normalized to unity absorbance at 532 nm), and the •OH generation abilities follow the order of **4** > **2** > **1** > **3** > HB > **5**, consistent with the trends of $O_2^{-\bullet}$. It is speculated that the hydroxyl radical is from the reaction $O_2^{-\bullet} + 2H_2O \rightarrow H_2O_2 + OH^- + \bullet OH$.[12c,34] The lowest •OH EPR signal of complex **5** also stems from its reaction with DMPO−OH, as shown in Figure S16 in the Supporting Information. The ability of **3** to generate $O_2^{-\bullet}$ and •OH is inferior to that of **1** and **2**; however, its photo nuclease activity is much superior to that of **1** and **2**, demonstrating further the importance of the high binding affinity, which may greatly enhance the bioavailability of ROS.

(32) Hu, Y.; Jiang, L. *Chin. Sci. Bull.* **1996**, *41*, 229–232.
(33) Lang, K.; Wagnerova, M.; Stopka, P.; Dameran, W. *J. Photochem. Photobiol. A* **1992**, *67*, 187–195.
(34) Detmer, C. A.; Pamatong, F. V.; Bocarsly, J. R. *Inorg. Chem.* **1996**, *35*, 6292–6298.

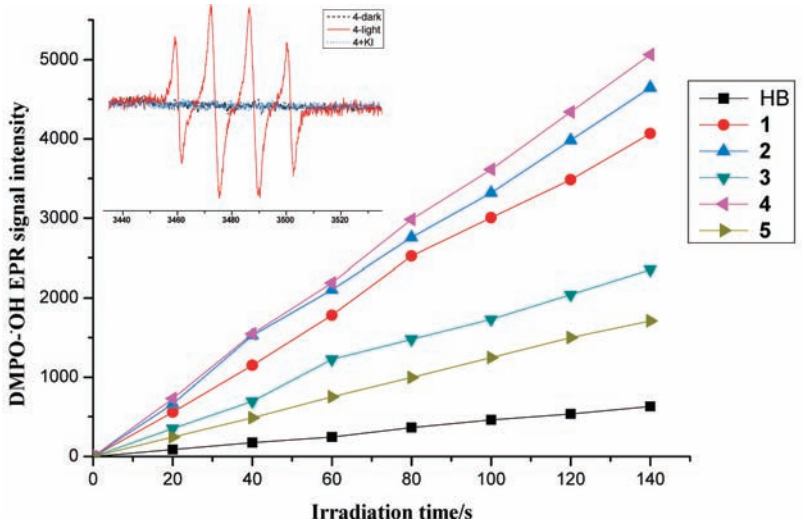

Figure 10. EPR signal intensity of DMPO-··OH as the function of irradiation time. The inset shows the EPR spectrum of DMPO-•OH obtained upon irradiation of air-saturated CH_3CN-H_2O (90:10 in volume ratio) solution of complex **4** (1 mM) and DMPO (50 mM) with 532 nm laser.

The reaction of $^1O_2$ with DPBF was adopted to measure the $^1O_2$ generation ability,[35] using HB as reference whose $^1O_2$ quantum yield was measured to be 0.76.[6] Upon irradiation (with the light of 500 nm obtained from a Hitachi F-4500 fluorescence spectrophotometer, 5 nm of excitation slit width) of the solutions of DPBF in the presence of complexes **1**−**5**, the fluorescence intensity of DPBF (λ_{ex} = 405 nm) did not change, indicating poor $^1O_2$ generation abilities of the complexes. In contrast, DPBF fluorescence intensity decreased greatly after irradiation in the presence of HB. We also used the EPR technique to compare the $^1O_2$ generation abilities of HB and the complexes, using TEMP (2,2,6,6-tetramethyl-4-piperidone) as spin-trapping agent. Irradiation with 532 nm laser of the HB solution containing TEMP led to a three-line EPR signal with a hyperfine splitting constant of 16.0 G, attributable to the adduct of TEMP and $^1O_2$.[10] In the cases of the complexes, no EPR signal can be detected, further indicating the poor $^1O_2$ generation abilities of complexes **1**−**5**. Clearly, the coordination of Cu^{2+} to HB switches the photodynamic activity from type II mechanism to type I mechanism, mainly because of the redox active nature of Cu^{2+}.

(35) Young, R. H.; Wehrly, K.; Martin, R. L. *J. Am. Chem. Soc.* **1971**, *93*, 5774–5779.

4. Conclusion

In summary, five new HB complexes based on redox-active Cu^{2+} ion were designed and synthesized for PDT application. Compared to HB, the Cu^{2+}-HB complexes exhibit improved water solubility, enhanced absorptivity in the phototherapeutic window, and increased binding affinity toward dsDNA. The readily available redox potential of Cu(II)/Cu(I) couple switches the photodynamic activity from type II mechanism (singlet oxygen mechanism) for HB to type I mechanism (radical mechanism) for the Cu^{2+}-HB complexes. Of the five Cu^{2+}-HB complexes, complexes **3**−**5** with terminal diimine ligands of tmp, dpq, and dppz, respectively, can photocleave supercoiled pBR322 DNA more efficiently than HB. These findings open a new avenue for the development of the HB derivatives with higher photodynamic activity and better clinical applicability.

Acknowledgment. This work was financially supported by NNSFC (20772133, 20873170) and CAS (KJCX2. YW.H08).

Supporting Information Available: Powder EPR spectra, photochemical stability examination, cyclic voltammograms, absorption titration, EB displacement assay, control experiments on DNA cleavage, MTT assay, and EPR spectra of DMPO−OH adduct (PDF). This material is available free of charge via the Internet at http://pubs.acs.org.